


Effects of cold and hot nuclear matter on J/ψ production at energies selected for the beam energy scan at the BNL Relativistic Heavy Ion Collider

Jiaxing Zhao  and Pengfei Zhuang 

Physics Department, Tsinghua University, Beijing 100084, China



(Received 28 February 2022; accepted 3 June 2022; published 13 June 2022)

Transverse momentum integrated and differential J/ψ R_{AA} are systematically studied in Au-Au collisions at energies selected for the beam energy scan at the BNL Relativistic Heavy Ion Collider using a transport approach, including cold and hot nuclear effects respectively in the initial conditions and the collision terms. With decreasing energy, while the temperature, lifetime, and size of the quark-gluon plasma (QGP) fireball decrease, the nuclear absorption of the initially produced charmonia is more and more strong, and the nuclear shadowing effect on charmonium regeneration goes to antishadowing first and then to shadowing again. As a competition between the cold and hot nuclear effects, the QGP phase is still important for charmonium production at $\sqrt{s_{NN}} = 200, 62.4, 54.4$ and 39 GeV but becomes negligible at $\sqrt{s_{NN}} = 14.5$ GeV.

DOI: [10.1103/PhysRevC.105.064907](https://doi.org/10.1103/PhysRevC.105.064907)

I. INTRODUCTION

It is widely accepted that a new state of matter, the so-called quark-gluon plasma (QGP), can be created in relativistic nuclear collisions. At extremely high colliding energy, as in collisions at the CERN Large Hadron Collider (LHC) and the BNL Relativistic Heavy Ion Collider (RHIC), the high temperature properties of the QGP have been systematically studied for decades [1,2]. Among the signatures of hot QGP, J/ψ has long been considered as a sensitive hard probe [3]. The competition between suppression due to color screening and regeneration due to quark coalescence can explain almost all the experimentally measured J/ψ data at low and intermediate momenta, including the nuclear modification factor R_{AA} [4–10] and collective flows v_2 [9–12] and v_3 [13].

The high density behavior of the QGP is still an open question and is the main subject of the Beam Energy Scan program at RHIC (RHIC-BES) [14]. When the colliding energy goes down, the lifetime, size, and temperature of the produced QGP are all reduced, but on the other hand the cold nuclear matter effect on charmonium production becomes significant. For instance, the nuclear absorption is enhanced because of the longer collision time [15], and the nuclear effect on parton distribution goes from shadowing to antishadowing with decreasing energy in the RHIC-BES region [16]. When the colliding energy is low enough, the hot medium may disappear and the cold nuclear effect will dominant charmonium production, as the case in proton-

nucleus collisions [17–19]. Considering the high statistics at RHIC-BES [20] and the canonical enhancement effect on charmonium production [17,21], one may precisely distinguish between the cold and hot nuclear matter effects. In this paper we focus on the cold and hot medium effects on J/ψ production in the RHIC-BES energy region in a transport approach.

II. J/ψ TRANSPORT IN QGP

The charmonium motion in phase space can be described by a transport equation including both initial production via hard processes and regeneration in a hot medium. The charmonium distribution $f_\psi(\mathbf{p}, x)$ for $\psi = J/\psi, \chi_c, \psi'$ in a phase-space cell with momentum \mathbf{p} and space-time coordinate $x = (t, \mathbf{x})$ is controlled by a relativistic Boltzmann transport equation,

$$p^\mu \partial_\mu f_\psi = -C_{\text{loss}} f_\psi + C_{\text{gain}}. \quad (1)$$

The hot nuclear effect, namely the charmonium suppression and regeneration in the created hot medium, is reflected in the loss term C_{loss} and gain term C_{gain} . Considering that the medium effect in the QGP phase is much stronger than that in the following hadron phase even at lower colliding energies [22], we do not take the hadron phase into account in this work. In this case the anomalous suppression comes from the charmonium melting in the hot QCD medium via Debye screening [23] and scattering with the surrounding partons [24–26]. Due to the Debye screening, the interaction range between a pair of charm quarks becomes shorter and shorter, and the bound state ($c\bar{c}$) will disappear sequentially [27]. This gives the dissociation temperatures $T_d \simeq (2.3, 1.2, 1.1)T_c$ for $J/\psi, \chi_c,$ and ψ' . If we take into account only the color screening, the temperature behavior of the dissociation is like a step function controlled by T_d : there is no dissociation for $T < T_d$ and the dissociation becomes

Published by the American Physical Society under the terms of the [Creative Commons Attribution 4.0 International](https://creativecommons.org/licenses/by/4.0/) license. Further distribution of this work must maintain attribution to the author(s) and the published article's title, journal citation, and DOI. Funded by SCOAP³.

infinity for $T \geq T_d$. This sudden dissociation is of course not the real case in heavy ion collisions where the dissociation is by the collisions between the quarkonia and the constituents of the medium. In the collision picture, the dissociation happens at any temperature including $T < T_d$ and $T \geq T_d$, and the dissociation rate should continuously increase with temperature. The dynamic scattering includes gluon dissociation and inelastic scatterings. In this paper, we consider the gluon dissociation $g + \psi \rightarrow c + \bar{c}$ as the dominant dissociation process in the QGP with $T < T_d$ and still take the dissociation rate to be infinity at $T \geq T_d$.

The dissociation cross section $\sigma_{g\psi}^{c\bar{c}}$ included in the loss term C_{loss} can be derived through the operator production expansion method and was calculated first by Peskin and Bhanot [25,26]. For instance, for the ground state the cross section is $\sigma_{g\psi}^{c\bar{c}} = A(r-1)^{3/2}/r^5$ with $A = 2^{11}\pi/(27\sqrt{m_Q^3\epsilon_\psi})$ and $r = \omega/\epsilon_\psi$, where m_Q is the heavy quark mass, m_ψ and ϵ_ψ are the charmonium mass and binding energy, s is the center-of-mass energy, and $\omega = (s - m_\psi^2)/(2m_\psi)$ is the gluon energy. The temperature and baryon chemical potential dependence of the binding energy can be determined by the two-body Schrödinger equation in medium [28]. In our numerical calculation here we simply take $\epsilon_\psi = 150$ MeV [6], which is smaller than its vacuum value.

Considering the inverse process $c + \bar{c} \rightarrow \psi + g$ for the gain term, the dissociation and regeneration rates $\alpha = C_{\text{loss}}/E$ and $\beta = C_{\text{gain}}/E$ are related to each other via detailed balance principal and can be expressed as [28]

$$\begin{aligned} \alpha(\mathbf{p}, x) &= \frac{1}{2E} \int \frac{d^3\mathbf{p}_g}{(2\pi)^3 2E_g} W_{g\psi}^{c\bar{c}}(s) f_g(\mathbf{p}_g, x) \\ &\quad \times \Theta(T(x) - T_c), \\ \beta(\mathbf{p}, x) &= \frac{1}{2E} \int \frac{d^3\mathbf{p}_g}{(2\pi)^3 2E_g} \frac{d^3\mathbf{p}_c}{(2\pi)^3 2E_c} \frac{d^3\mathbf{p}_{\bar{c}}}{(2\pi)^3 2E_{\bar{c}}} \\ &\quad \times F_c F_r W_{c\bar{c}}^{g\psi}(s) f_c(\mathbf{p}_c, x) f_{\bar{c}}(\mathbf{p}_{\bar{c}}, x) \\ &\quad \times \Theta(T(x) - T_c) (2\pi)^4 \delta(p + p_g - p_c - p_{\bar{c}}), \quad (2) \end{aligned}$$

where $W_{g\psi}^{c\bar{c}}(s)$ is the dissociation probability constructed by the cross section $\sigma_{g\psi}^{c\bar{c}}(s)$ and related to the regeneration probability $W_{c\bar{c}}^{g\psi}(s)$ via detailed balance, and $p = (E, \mathbf{p})$, $p_g = (E_g, \mathbf{p}_g)$, $p_c = (E_c, \mathbf{p}_c)$, and $p_{\bar{c}} = (E_{\bar{c}}, \mathbf{p}_{\bar{c}})$ are charmonium, gluon, charm quark and anticharm quark four-momenta. The step function $\Theta(T(x) - T_c)$ means that we consider here only the charmonium suppression and regeneration in the QGP phase, where T_c is the deconfinement phase transition temperature determined by the equation of state of the system. The space-time evolution of the medium temperature $T(x)$ is solved from the hydrodynamics, which will be discussed in the next section.

Since gluons are a kind of constituent of the QGP, the gluon distribution is taken as the Bose-Einstein function $f_g = 1/(e^{p \cdot u/T} - 1)$ with local temperature $T(x)$ and velocity $u_\mu(x)$ of the medium controlled by the hydrodynamics. Considering the energy loss during the motion, the charm quark distribution should be controlled by a transport approach and lie in between two limits: the perturbative QCD limit without

interaction with the medium and the thermalization limit via strong interaction with the medium. From the experimentally observed large charmed meson flow in Au-Au collisions at $\sqrt{s_{NN}} = 200$ GeV [29], charm quarks seem to be thermalized at top RHIC and LHC energies, and we can take, as a first approximation, a kinetically equilibrated distribution for charm (anticharm) quarks $f_c = \rho_c(x)N(x)/(e^{p \cdot u/T} + 1)$ with the local normalization factor $N(x)$. Considering the lower temperature and shorter QGP lifetime in nuclear collisions at RHIC-BES energies, charm quarks may not fully thermalized. The partial thermalization can be described by introducing a relaxation factor [30–32]

$$F_r = 1 - e^{-\tau/\tau_r}, \quad (3)$$

where $\tau = \sqrt{t^2 - z^2}$ is the proper time which together with the longitudinal space-time rapidity $\eta = 1/2 \ln[(t-z)/(t+z)]$ are usually used to replace t and z . The relaxation time τ_r characterizes the averaged thermalization time of the medium, and we take $\tau_r \simeq 7$ fm/c [33] at RHIC-BES energies. Considering the fact that higher momentum particles will be enhanced in a pQCD distribution in comparison with a thermal distribution, the obtained charmonium distribution will be shifted to higher transverse momentum, when we take the limit of perturbative QCD distribution for charm quarks. The detailed calculation and discussion are given in Refs. [9,12].

The other effect on charm quark distribution at high baryon density is the canonical enhancement. When only a few pairs of charm quarks are produced in an event, the charm conservation effect within the canonical ensemble needs to be considered. It becomes significant and enhances charmonium production in heavy ion collisions at lower energies. If the charm quark pairs are produced at the same rapidity, the canonical enhancement factor for charmonium production can be simply parametrized as [17,21,34,35]

$$F_c = 1 + \frac{1}{dN_{c\bar{c}}/dy}, \quad (4)$$

controlled by the number of directly produced $c\bar{c}$ pairs. We take $dN_{c\bar{c}}/dy = 1.31$ and 0.027 in Au-Au collisions with centrality bin 0–60% at $\sqrt{s_{NN}} = 200$ and 14.5 GeV, the corresponding canonical factor is 1.76 and 38.4. The charmonium enhancement is really dramatic in lower energy nuclear collisions. The charm quark density $\rho_c(x)$ in coordinate space is controlled by the charm conservation equation $\partial_\mu(\rho_c u^\mu) = 0$. Since charm quarks at RHIC-BES energies are all produced via initial binary collisions and move freely in the prehydro stage, the initial density is governed by the nuclear geometry,

$$\rho_c(\mathbf{x}, \tau_0) = \frac{\mathcal{T}_A(\mathbf{x}_T + \frac{\mathbf{b}}{2}) \mathcal{T}_B(\mathbf{x}_T - \frac{\mathbf{b}}{2}) \cosh \eta \, d\sigma_{pp}^{c\bar{c}}}{\tau_0 \, d\eta}, \quad (5)$$

where \mathcal{T}_A and \mathcal{T}_B are the thickness functions for the two colliding nuclei A and B [36],

$$\begin{aligned} \mathcal{T}_{A/B}(\mathbf{x}_T) &= T_{A/B}(\mathbf{x}_T, -\infty, +\infty), \\ \mathcal{T}_{A/B}(\mathbf{x}_T, z_i, z_j) &= \int_{z_i}^{z_j} \rho_{A/B}(\mathbf{x}_T, z) dz \quad (6) \end{aligned}$$

with $\rho_{A/B}$ being the nuclear matter distribution in the two colliding nuclei, \mathbf{x}_T is the transverse coordinate, \mathbf{b} is the impact

TABLE I. The values of the parameters used to describe the initial medium (τ_0 , s_0 , σ_{pp}^m), initial charmonium distribution ($d\sigma_{pp}^{J/\psi}/dy$, $\langle p_T^2 \rangle$, $d\sigma_{pp}^{c\bar{c}}/dy$), and cold nuclear matter effect ($\sigma_{abs}^{J/\psi}$, a_{gN}) at RHIC-BES energies.

$\sqrt{s_{NN}}$ (GeV)	τ_0 (fm/c)	s_0	σ_{pp}^{in} (mb)	$d\sigma_{pp}^{J/\psi}/dy$ (nb)	$\langle p_T^2 \rangle$ (GeV) ²	$d\sigma_{pp}^{c\bar{c}}/dy$ (μ b)	$\sigma_{abs}^{J/\psi}$ (mb)	a_{gN} (GeV ² /fm)
200	0.6	9.3	41	716.7	3.05	162.0	1.5	0.100
62.4	1.0	10.8	36	295.7	1.85	45.0	4.8	0.085
54.4	1.1	10.5	35	252.0	1.74	38.3	5.0	0.085
39	1.3	10.35	34	150.7	1.46	27.5	5.2	0.080
14.5	2.2	9.22	32	37.6	0.77	3.3	8.9	0.077

parameter of the nuclear collisions, and $d\sigma_{pp}^{c\bar{c}}/d\eta$ is the rapidity distribution of charm quark production cross section in p - p collisions [37–39]. The value of $d\sigma_{pp}^{c\bar{c}}/d\eta$ at RHIC-BES energies is shown in Table I.

The initial charmonium distribution for the transport equation (1) can be obtained from a superposition of p - p collisions, along with the modifications from several cold nuclear effects. The J/ψ momentum distribution in p - p collisions can be factorized as [40],

$$\frac{d^2\sigma_{pp}^{J/\psi}}{2\pi p_T dp_T dy} = \frac{a}{2\pi \langle p_T^2 \rangle} \left(1 + b^2 \frac{p_T^2}{\langle p_T^2 \rangle} \right)^{-n} \frac{d\sigma_{pp}^{J/\psi}}{dy} \quad (7)$$

with parameters $a = 2b^2(n-1)$, $b = \Gamma(3/2)\Gamma(n-3/2)/\Gamma(n-1)$, and $n = 3.93 \pm 0.03$. Taking the averaged momentum squared and differential cross section shown in Table I, the J/ψ transverse momentum distribution in p - p collisions at midrapidity is plotted in Fig. 1 at RHIC-BES energies and compared with the experimental data at $\sqrt{s_{NN}} = 200$ GeV.

The cold nuclear effect usually consists of nuclear shadowing [43], Cronin effect [44,45], and nuclear absorption [46]. Unlike the collisions at LHC energy and top RHIC energy, the nuclear collision time at RHIC-BES energies is comparable with or even longer than the charmonium formation time; the produced charmonia will be sizeably absorbed by the surrounding nuclear matter. The surviving probability after

the absorption can be expressed as

$$S_{abs} = e^{-\sigma_{abs}[T_A(x_T + \frac{b}{2}, z_A, \infty) + T_B(x_T - \frac{b}{2}, -\infty, z_B)]}, \quad (8)$$

where z_A and z_B are the longitudinal coordinates of the charmonium production point in the local rest frames of the two colliding nuclei. The absorption cross section $\sigma_{abs}^{J/\psi}$ for the ground state J/ψ is fixed by fitting the experimental data [15]; see Table I. For the excited states, the experimental data are still rare. Neglecting the difference in formation time, the absorption cross sections for the excited states can be obtained from $\sigma_{abs}^{J/\psi}$ through the mean-square-radius scaling law,

$$\sigma_{abs}^{\psi} = \frac{\langle r_{\psi}^2 \rangle}{\langle r_{J/\psi}^2 \rangle} \sigma_{abs}^{J/\psi}, \quad (9)$$

where the mean-square radius can be obtained by solving the two-body Schrödinger equation with the Cornell potential [28], which leads to $\langle r_{J/\psi}^2 \rangle = 0.239$ fm², $\langle r_{\chi_c}^2 \rangle = 0.510$ fm², and $\langle r_{\psi(2S)}^2 \rangle = 0.808$ fm².

Before two gluons fuse into a charmonium, they acquire additional transverse momentum via multiscattering with the surrounding nucleons, and this extra momentum would be inherited by the produced charmonium; this is called Cronin effect [44,45]. Therefore, when doing the superposition of the p - p distribution (7), we should make the replacement of $\langle p_T^2 \rangle$ by [47]

$$\langle p_T^2 \rangle + a_{gN}l, \quad (10)$$

where the Cronin parameter a_{gN} is the averaged charmonium transverse momentum square obtained from the gluon scattering with a unit of length of nucleons, and l is the mean trajectory length of the two gluons in the two nuclei before the $c\bar{c}$ formation. The experimentally measured averaged momentum square for J/ψ in p - A collisions at Super Proton Synchrotron (SPS) energy and d -Au collisions at top RHIC energy can be well described by the Cronin effect [48,49]. The values of a_{gN} at RHIC-BES energies are shown in Table I. To smooth the Cronin effect, we take in numerical calculations a Gaussian smearing [5,47] for the modified transverse momentum distribution.

The shadowing effect modifies the parton distribution in a nucleus relative to that in a nucleon, which changes the open and hidden charm yields in nuclear collisions [50,51]. The effect is mainly due to the parton collectivity in a nucleus [52] and can be parametrized as a modification factor $\mathcal{R}_i = \bar{f}_i(x, \mu_F)/[Af_i(x, \mu_F)]$, where \bar{f}_i and f_i are the parton distribution functions (i = gluon, light, strange, and heavy

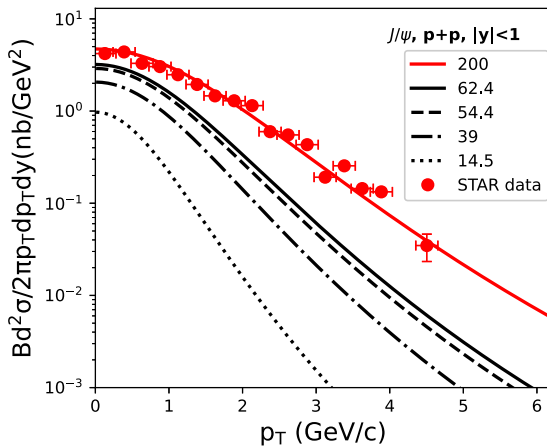


FIG. 1. The J/ψ p_T distribution at midrapidity in p - p collisions at RHIC-BES energies. The experiment data at $\sqrt{s_{NN}} = 200$ GeV are from Ref. [41], and $B(J/\psi \rightarrow e^+e^-) = 5.97 \pm 0.03\%$ [42] is the branch ratio.

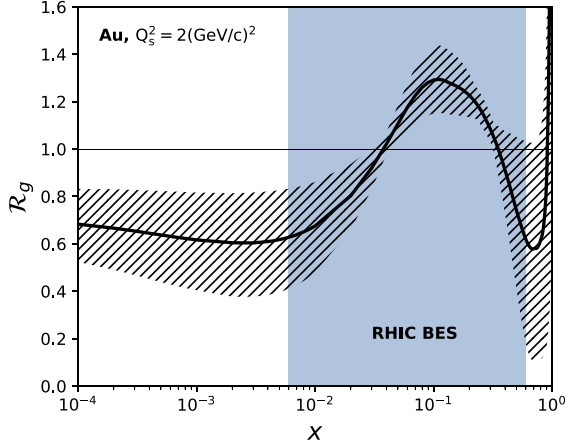


FIG. 2. The nuclear modification factor \mathcal{R}_g for gluons in nucleus Au from the EPS09 NLO model [16]. The solid line inside the slashed band indicates the central value of the shadowing effect, and the vertical band shows the momentum fraction range covered by RHIC-BES energies for two gluons to produce a J/ψ .

quarks) in a nucleus and a free nucleon, x is the longitudinal momentum fraction, and the factorization scale is taken as $\mu_F = \sqrt{m_\psi^2 + p_T^2}$. The modification factor can be simulated by, for instance, the EPS09 package [16], as shown in Fig. 2 for gluons. The interesting point here is the x dependence of the shadowing effect at RHIC-BES energies. A simple estimation of the longitudinal momentum fraction x of the two initial gluons in this energy region is in the range of $0.006 < x < 0.607$; see the vertical band in Fig. 2. Around and above the top RHIC energy, there is always shadowing effect with $\mathcal{R}_g < 1$, while in the RHIC-BES region the shadowing approaches antishadowing when the colliding energy decreases. This change of shadowing effect may significantly affect the charmonium production in nuclear collisions.

Including the above discussed nuclear absorption, Cronin effect and shadowing effect, the initial charmonium distribution can be written as

$$\begin{aligned}
 f_\psi(\mathbf{p}, \mathbf{x}, \tau_0) &= \frac{(2\pi)^3}{E\tau_0} \int dz_A dz_B \rho_A\left(\mathbf{x}_T + \frac{\mathbf{b}}{2}, z_A\right) \rho_B\left(\mathbf{x}_T - \frac{\mathbf{b}}{2}, z_B\right) \\
 &\times S_{abs} \mathcal{R}_g\left(x_1, \mu_F, \mathbf{x}_T + \frac{\mathbf{b}}{2}\right) \mathcal{R}_g\left(x_2, \mu_F, \mathbf{x}_T - \frac{\mathbf{b}}{2}\right) \\
 &\times f_\psi^{pp}(\mathbf{p}, \mathbf{x}, z_A, z_B), \quad (11)
 \end{aligned}$$

where, from the momentum conservation, the longitudinal momentum fractions of the two initial gluons are fixed to be $x_{1,2} = \sqrt{m_\psi^2 + p_T^2} / \sqrt{s_{NN}} e^{\pm y}$ with y being the charmonium rapidity.

III. EVOLUTION OF QGP

The quark matter created in high energy nuclear collisions is a very perfect fluid [53,54] and its space-time evolution can be simulated by hydrodynamics with the conservation

equations of energy-momentum and net baryon density,

$$\partial_\mu T^{\mu\nu} = 0, \quad \partial_\mu J_B^\mu = 0. \quad (12)$$

The energy-momentum tensor $T^{\mu\nu}$ and net baryon current J_B^μ are expressed as

$$\begin{aligned}
 T^{\mu\nu} &= \epsilon u^\mu u^\nu - (P + \Pi)\Delta^{\mu\nu} + \pi^{\mu\nu}, \\
 J_B^\mu &= n_B u^\mu + q^\mu,
 \end{aligned} \quad (13)$$

where ϵ is the medium energy density, P the pressure, Π the bulk viscous pressure, $\Delta^{\mu\nu} = g^{\mu\nu} - u^\mu u^\nu$ the projection tensor, $\pi^{\mu\nu}$ the shear stress tensor, n_B the net baryon density, and q^μ the baryon diffusion current. In the following calculation, we take the ratio of shear viscosity to entropy density as a constant, $\eta/s = 0.08$, and neglect the bulk viscosity and baryon diffusion. To close the hydrodynamic equations, we use NEOS-B as the equation of state at finite baryon chemical potential [55,56].

The initial condition of the hydrodynamic equations, such as the initial entropy density and baryon density, can be obtained from the assumption that they come independently from the two colliding nuclei [57],

$$\begin{aligned}
 s(\mathbf{x}, \tau_0) &= \frac{s_0}{\tau_0} [f_P^s(\eta) N_P(\mathbf{x}_T) + f_T^s(\eta) N_T(\mathbf{x}_T)], \\
 n_B(\mathbf{x}, \tau_0) &= \frac{1}{\tau_0} [f_P^n(\eta) N_P(\mathbf{x}_T) + f_T^n(\eta) N_T(\mathbf{x}_T)],
 \end{aligned} \quad (14)$$

where s_0 is the maximum entropy density, which is adjusted to reproduce the experimentally observed multiplicity, and f_P^s, f_P^n and f_T^s, f_T^n are rapidity distributions of the initial entropy and baryon number produced by the projectile and target nuclei. Since the initial entropy mainly comes from the ‘‘soft’’ processes in low energy nuclear collisions [58], the number of participating nucleons is the number of sources to produce entropy and baryon number N_P and N_T , which can be calculated through the optical Glauber model [57,59],

$$\begin{aligned}
 N_P(\mathbf{x}_T) &= \mathcal{T}_A\left(\mathbf{x}_T + \frac{\mathbf{b}}{2}\right) (1 - e^{-\sigma_{pp}^{in} \mathcal{T}_B(\mathbf{x}_T - \frac{\mathbf{b}}{2})}), \\
 N_T(\mathbf{x}_T) &= \mathcal{T}_B\left(\mathbf{x}_T - \frac{\mathbf{b}}{2}\right) (1 - e^{-\sigma_{pp}^{in} \mathcal{T}_A(\mathbf{x}_T + \frac{\mathbf{b}}{2})}). \quad (15)
 \end{aligned}$$

The values of the inelastic scattering cross section σ_{pp}^{in} in p - p collisions which can be obtained through theoretical calculation and experimental measurement [60,61], the initial time τ_0 of the medium which can be estimated from the overlap time of the two colliding nuclei [62,63], and the maximum entropy density s_0 at RHIC-BES energies are listed in Table I.

The hydrodynamic equations with the above initial condition can be numerically solved with the help of the MUSIC package [57,64]. The time evolution of the temperature at the center of the QGP medium created in central Au-Au collisions at RHIC-BES energies is shown in Fig. 3. Considering the expansion of the fluid, the temperature decreases monotonically with time. While the thermalization time (initial time) of the system is different at different colliding energies, the evolution trajectory of the temperature is almost the same for all the energies. It starts at the maximum temperature at initial time τ_0 and ends at the critical temperature T_c of the QGP. The

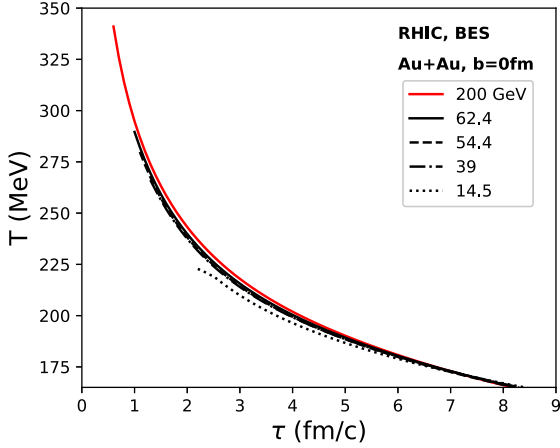


FIG. 3. The temperature evolution at the center of the QGP medium created in central Au-Au collisions at RHIC-BES energies.

maximum temperatures for colliding energies $\sqrt{s_{NN}} = 200, 62.4, 54.4, 39,$ and 14.5 GeV are 321.0, 289.6, 279.8, 266.1, and 244.5 MeV, and the critical temperature $T_c = 165$ MeV is almost colliding energy independent [65,66]. Since the QGP phase is formed even at $\sqrt{s_{NN}} = 14.5$ GeV, we can use the transport equation (1) to describe charmonium motion in nuclear collisions at RHIC-BES energies.

IV. RESULTS

The Boltzmann equation (1), with cold nuclear effect in the initial condition (11) and hot nuclear effect in the collision terms (2), can be analytically solved [6,28]. As a ground state of $c\bar{c}$, the experimentally observed J/ψ 's contain the direct production and the decay contribution from the excited states and B hadrons. Since the B decay is mainly in the high p_T region and becomes important at LHC energy, we neglect it for nuclear collisions at RHIC-BES energies. For the feed-down, we take 22% of χ_c 's and 61% of ψ 's to decay to J/ψ 's in this energy region [42]. We focus in this section on the J/ψ nuclear modification factor $R_{AA} = N_{AA}/(N_{coll}N_{pp})$, where N_{pp} and N_{AA} are the J/ψ numbers produced in p - p and Au-Au collisions, and N_{part} and N_{coll} are the number of participating nucleons and the number of binary collisions. All the calculations are at midrapidity.

The centrality dependence of R_{AA} and its transverse momentum distribution in a fixed centrality bin 0–60% at RHIC top energy $\sqrt{s_{NN}} = 200$ GeV are shown in Fig. 4. The slashed bands are the calculations considering only cold nuclear effect ($\alpha = \beta = 0$). The band structure is due to the uncertainty of the shadowing effect shown in Fig. 2. The full result with both cold and hot nuclear effects is plotted as the crossed bands, where the shadowing effect is taken as its central value indicated by the solid line in Fig. 2. The upper and lower limits of the bands are the calculations with and without considering the canonical enhancement factor F_c . Since the canonical effect influences only the regeneration process in peripheral collisions, it becomes important at lower N_{part} and lower p_T . At high p_T , the regeneration contribution and in turn the canonical enhancement disappears, and the band approaches

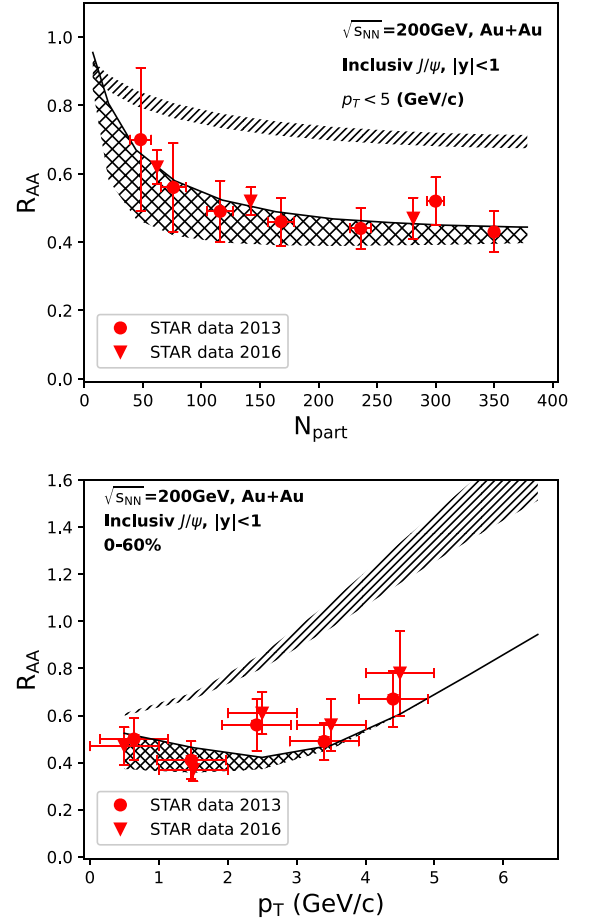


FIG. 4. The nuclear modifications factor R_{AA} for inclusive J/ψ 's as a function of N_{part} (upper panel) and p_T (lower panel) in Au-Au collisions at top RHIC energy $\sqrt{s_{NN}}=200$ GeV. The slashed and crossed bands are the calculations with only cold nuclear effect and with both cold and hot nuclear effects. The experimental data are from the STAR collaboration [20,67].

being a line. The competition between the two aspects of the hot nuclear effect, namely the suppression and regeneration, lowers the charmonium yield. From the comparison with the experimental data [20,67], the QGP effect, which is the difference between the slashed and crossed bands, is significant at RHIC top energy.

We now turn to see the energy dependence of charmonium production. The J/ψ nuclear modification factor R_{AA} as a function of centrality N_{part} and transverse momentum p_T are displayed in Figs. 5 and 6 at colliding energies $\sqrt{s_{NN}} = 62.4, 54.4, 39,$ and 14.5 GeV. Again the slashed and crossed bands are the calculations with only cold nuclear effect and with both cold and hot nuclear effects. When the colliding energy decreases from 62.4 to 54.4 and then to 39 GeV, the antishadowing effect becomes more and more strong, see Fig. 2, which enhances the charmonium production and compensates for the larger and larger nuclear absorption. As a result, the cold nuclear effect is almost the same at these three energies. When the energy decreases further, the antishadowing comes back to shadowing, and the averaged modification factor \mathcal{R}_g

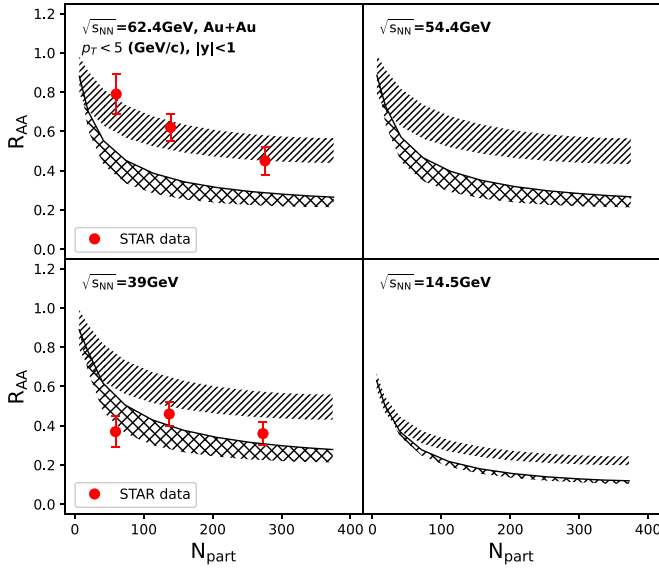


FIG. 5. The nuclear modifications factor R_{AA} for inclusive J/ψ 's as a function of N_{part} in Au-Au collisions at colliding energies $\sqrt{s_{NN}} = 62.4, 54.4, 39,$ and 14.5 GeV. The slashed and crossed bands are the calculations with only cold nuclear effect and with both cold and hot nuclear effects. The experimental data are from the STAR Collaboration [20].

at 14.5 GeV is slightly less than unity, and the strong nuclear absorption in this case leads to a strong J/ψ suppression. While the canonical enhancement factor F_c is extremely large at $\sqrt{s_{NN}} = 14.5$ GeV, its contribution to the total yield is very small; see the narrow bands in Figs. 5 and 6. This is due to the

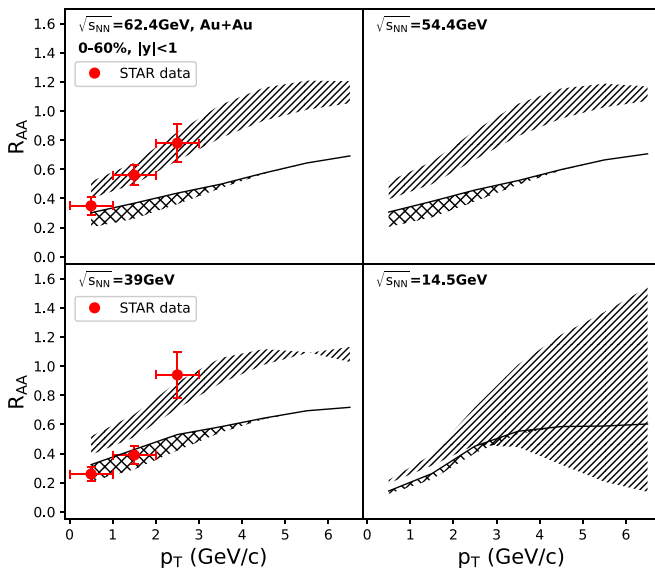


FIG. 6. The nuclear modifications factor R_{AA} for inclusive J/ψ 's as a function of p_T in Au-Au collisions at colliding energies $\sqrt{s_{NN}} = 62.4, 54.4, 39,$ and 14.5 GeV. The slashed and crossed bands are the calculations with only cold nuclear effect and with both cold and hot nuclear effects. The experimental data are from the STAR Collaboration [20].

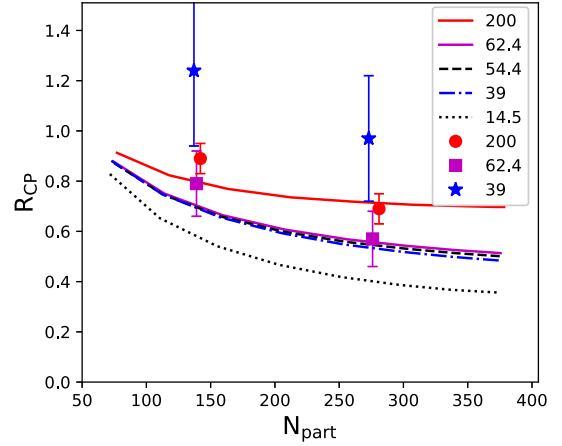


FIG. 7. The nuclear modification factor R_{CP} for inclusive J/ψ 's as a function of centrality in Au-Au collisions at RHIC-BES energies. A peripheral collision is defined as the collisions with centrality bin 40–60%, and the experimental data are from the STAR Collaboration [20].

fact that, the canonical effect modifies only the regeneration and the regeneration part becomes less and less important with decreasing colliding energy. At $\sqrt{s_{NN}} = 62.4, 54.4,$ and 39 GeV, the hot nuclear effect, namely the difference between the slashed and corresponding crossed bands, is still very clear, which indicates a sizable QGP formation in the collisions at these energies. However, when the colliding energy goes down to 14.5 GeV, the hot nuclear effect is already weak, the two bands in p_T distribution becomes indistinguishable due to the large uncertainty in the shadowing effect. From the comparison with the experimental data, the full calculation agrees reasonably well with the data at $\sqrt{s_{NN}} = 200$ and 39 GeV, but it deviates clearly from the data at $\sqrt{s_{NN}} = 62.4$ GeV, for both N_{part} and p_T distributions. It is strange that only the cold nuclear effect can explain the data very well at this intermediate energy, while the hot nuclear effect plays an important role at higher and lower energies. The case here is similar to other model calculations [5,20]. More precise theoretical and experimental study around this energy is needed.

Aiming to eliminate the uncertainty from p - p collisions, one usually defines the nuclear modification factor R_{CP} , which is a ratio of the particle yield in collisions with a given centrality bin to that in the peripheral collisions, $R_{CP} = ((dN/dy)/N_{coll})_b / ((dN/dy)/N_{coll})_{perp}$. For J/ψ , this is a quantity to describe the relative suppression in the two bins. If the medium effect is centrality independent, there is always $R_{CP} = 1$. With the above described cold and hot medium effects, R_{CP} as a function of centrality and the comparison with experimental data are shown in Fig. 7 for Au-Au collisions at RHIC-BES energies. The deviation from unity indicates clearly the sizable medium effect at these energies.

V. SUMMARY

Cold and hot nuclear matter effects are the driving force to study nuclear collisions at high energies. The former is the basement and the latter is the condition to form the

QGP, a new state of nuclear matter. At LHC and top RHIC energies, the cold nuclear effect is weak and the hot nuclear effect is the dominant one. For heavy ion collisions at RHIC-BEC energies, the cold nuclear effect becomes strong and the hot nuclear effect is still important, the competition between the two governs the charmonium production as a probe of the QGP. In this paper we take a transport equation, which can distinguish clearly the cold nuclear effect in the initial condition from the hot nuclear effect in the collision terms, to study transverse momentum integrated and differential J/ψ R_{AA} in Au-Au collisions at RHIC-BES energies.

With decreasing energy, more and more initially produced charmonia are absorbed by the surrounding nuclear matter, and the shadowing effect on charmonium regeneration be-

comes anti-shadowing first and then shadowing again. This change in nuclear absorption and shadowing leads to an almost energy-independent cold nuclear effect at $\sqrt{s_{NN}} = 62.4, 54.4$ and 39 GeV and a much stronger cold nuclear effect at $\sqrt{s_{NN}} = 14.5$ GeV. For the hot nuclear effect, the temperature, life time and size of the QGP fireball monotonously decrease with decreasing colliding energy. At $\sqrt{s_{NN}} = 14.5$ GeV the cold nuclear effect becomes the dominant one and the hot nuclear effect is negligible.

ACKNOWLEDGMENTS

The work is supported by Guangdong Major Project of Basic and Applied Basic Research No. 2020B0301030008 and NSFC Grant Nos. 11890712, 12075129, and 12175165.

-
- [1] J. Adams Jr. *et al.* (STAR Collaboration), *Nucl. Phys. A* **757**, 102 (2005).
- [2] B. Müller, J. Schukraft, and B. Wyslouch, *Annu. Rev. Nucl. Part. Sci.* **62**, 361 (2012).
- [3] T. Matsui and H. Satz, *Phys. Lett. B* **178**, 416 (1986).
- [4] X. Zhao and R. Rapp, *Nucl. Phys. A* **859**, 114 (2011).
- [5] X. Zhao and R. Rapp, *Phys. Rev. C* **82**, 064905 (2010).
- [6] Y. Liu, Z. Qu, N. Xu, and P. Zhuang, *J. Phys. G: Nucl. Part. Phys.* **37**, 075110 (2010).
- [7] X. Du and R. Rapp, *Nucl. Phys. A* **943**, 147 (2015).
- [8] J. Zhao and B. Chen, *Phys. Lett. B* **776**, 17 (2018).
- [9] K. Zhou, N. Xu, Z. Xu, and P. Zhuang, *Phys. Rev. C* **89**, 054911 (2014).
- [10] B. Chen, *Chin. Phys. C* **43**, 124101 (2019).
- [11] X. L. Zhu, P. F. Zhuang and N. Xu, *Phys. Lett. B* **607**, 107 (2005).
- [12] M. He, B. Wu and R. Rapp, *Phys. Rev. Lett.* **128**, 162301 (2022).
- [13] J. Zhao, B. Chen, and P. Zhuang, *Phys. Rev. C* **105**, 034902 (2022).
- [14] A. Bzdak, S. Esumi, V. Koch, J. Liao, M. Stephanov, and N. Xu, *Phys. Rep.* **853**, 1 (2020).
- [15] N. Brambilla, S. Eidelman, B. K. Heltsley, R. Vogt, G. T. Bodwin, E. Eichten, A. D. Frawley, A. B. Meyer, R. E. Mitchell, and V. Papadimitriou *et al.*, *Eur. Phys. J. C* **71**, 1534 (2011).
- [16] I. Helenius, K. J. Eskola, H. Honkanen, and C. A. Salgado, *J. High Energy Phys.* **07** (2012) 073.
- [17] Y. Liu, C. M. Ko, and T. Song, *Phys. Lett. B* **728**, 437 (2014).
- [18] B. Chen, T. Guo, Y. Liu, and P. Zhuang, *Phys. Lett. B* **765**, 323 (2017).
- [19] X. Du and R. Rapp, *J. High Energy Phys.* **03** (2019) 015.
- [20] L. Adamczyk, Jr. *et al.* (STAR Collaboration), *Phys. Lett. B* **771**, 13 (2017).
- [21] M. I. Gorenstein, A. P. Kostyuk, H. Stoecker, and W. Greiner, *Phys. Lett. B* **509**, 277 (2001).
- [22] B. Chen, *Phys. Rev. C* **93**, 044917 (2016).
- [23] S. Digal, O. Kaczmarek, F. Karsch, and H. Satz, *Eur. Phys. J. C* **43**, 71 (2005).
- [24] L. Grandchamp and R. Rapp, *Phys. Lett. B* **523**, 60 (2001).
- [25] M. E. Peskin, *Nucl. Phys. B* **156**, 365 (1979).
- [26] G. Bhanot and M. E. Peskin, *Nucl. Phys. B* **156**, 391 (1979).
- [27] H. Satz, *J. Phys. G: Nucl. Part. Phys.* **32**, R25 (2006).
- [28] J. Zhao, K. Zhou, S. Chen, and P. Zhuang, *Prog. Part. Nucl. Phys.* **114**, 103801 (2020).
- [29] L. Adamczyk *et al.* (STAR Collaboration), *Phys. Rev. Lett.* **118**, 212301 (2017).
- [30] L. Grandchamp, R. Rapp, and G. E. Brown, *Phys. Rev. Lett.* **92**, 212301 (2004).
- [31] T. Song, K. C. Han, and C. M. Ko, *Phys. Rev. C* **85**, 054905 (2012).
- [32] L. Grandchamp and R. Rapp, *Nucl. Phys. A* **709**, 415 (2002).
- [33] X. Zhao and R. Rapp, *Phys. Lett. B* **664**, 253 (2008).
- [34] A. Andronic, P. Braun-Munzinger, K. Redlich, and J. Stachel, *Nucl. Phys. A* **789**, 334 (2007).
- [35] A. P. Kostyuk, [arXiv:nucl-th/0502005](https://arxiv.org/abs/nucl-th/0502005) [nucl-th].
- [36] M. L. Miller, K. Reygers, S. J. Sanders, and P. Steinberg, *Annu. Rev. Nucl. Part. Sci.* **57**, 205 (2007).
- [37] B. Abelev *et al.* (ALICE Collaboration), *J. High Energy Phys.* **01** (2012) 128.
- [38] M. Cacciari, M. Greco, and P. Nason, *J. High Energy Phys.* **05** (1998) 007.
- [39] M. Cacciari, S. Frixione, and P. Nason, *J. High Energy Phys.* **03** (2001) 006.
- [40] W. Zha, B. Huang, R. Ma, L. Ruan, Z. Tang, Z. Xu, C. Yang, Q. Yang, and S. Yang, *Phys. Rev. C* **93**, 024919 (2016).
- [41] J. Adam, Jr. *et al.* (STAR Collaboration), *Phys. Lett. B* **786**, 87 (2018).
- [42] P. A. Zyla *et al.* (Particle Data Group), *PTEP* **2020**, 083C01 (2020).
- [43] A. H. Mueller and J. w. Qiu, *Nucl. Phys. B* **268**, 427 (1986).
- [44] J. Cronin, H. J. Frisch, M. Shochet, J. Boymond, R. Mermod, P. Piroue, and R. L. Sumner, *Phys. Rev. D* **11**, 3105 (1975).
- [45] J. Hüfner, Y. Kurihara, and H. J. Pirner, *Phys. Lett. B* **215**, 218 (1988).
- [46] C. Gerschel and J. Hüfner, *Phys. Lett. B* **207**, 253 (1988).
- [47] J. Hüfner and P. F. Zhuang, *Phys. Lett. B* **559**, 193 (2003).
- [48] N. S. Topilskaya *et al.* (NA50 Collaboration), *Nucl. Phys. A* **715**, 675c (2003).
- [49] A. Adare *et al.* (PHENIX Collaboration), *Phys. Rev. C* **77**, 024912 (2008); **79**, 059901(E) (2009).
- [50] S. Gavin, P. L. McGaughey, P. V. Ruuskanen, and R. Vogt, *Phys. Rev. C* **54**, 2606 (1996).
- [51] R. Vogt, *Phys. Rev. C* **81**, 044903 (2010).

- [52] P. Norton, [Rep. Prog. Phys.](#) **66**, 1253 (2003).
- [53] D. Teaney, [Phys. Rev. C](#) **68**, 034913 (2003).
- [54] R. A. Lacey, N. N. Ajitanand, J. M. Alexander, P. Chung, W. G. Holzmann, M. Issah, A. Taranenko, P. Danielewicz, and H. Stöcker, [Phys. Rev. Lett.](#) **98**, 092301 (2007).
- [55] A. Monnai, B. Schenke, and C. Shen, [Phys. Rev. C](#) **100**, 024907 (2019).
- [56] A. Monnai, B. Schenke, and C. Shen, [Int. J. Mod. Phys. A](#) **36**, 2130007 (2021).
- [57] G. S. Denicol, C. Gale, S. Jeon, A. Monnai, B. Schenke, and C. Shen, [Phys. Rev. C](#) **98**, 034916 (2018).
- [58] D. Kharzeev and M. Nardi, [Phys. Lett. B](#) **507**, 121 (2001).
- [59] X.-Y. Wu, G.-Y. Qin, L.-G. Pang, and X.-N. Wang, [Phys. Rev. C](#) **105**, 034909 (2022).
- [60] B. Abelev *et al.* (ALICE Collaboration), [Eur. Phys. J. C](#) **73**, 2456 (2013).
- [61] T. Sjöstrand, S. Mrenna, and P. Z. Skands, [J. High Energy Phys.](#) **05** (2006) 026.
- [62] C. Shen and B. Schenke, [Phys. Rev. C](#) **97**, 024907 (2018).
- [63] C. Shen and B. Schenke, [PoS CPOD2017](#), 006 (2018).
- [64] B. Schenke, S. Jeon, and C. Gale, [Phys. Rev. C](#) **82**, 014903 (2010).
- [65] A. Andronic, P. Braun-Munzinger, and J. Stachel, [Phys. Lett. B](#) **673**, 142 (2009); **678**, 516(E) (2009).
- [66] J. Cleymans, H. Oeschler, K. Redlich, and S. Wheaton, [Phys. Rev. C](#) **73**, 034905 (2006).
- [67] L. Adamczyk, Jr. *et al.* (STAR Collaboration), [Phys. Lett. B](#) **722**, 55 (2013).